The Journal of the Korean Society of
Coastal and Ocean Engineers
Vol. 5, No. 4, pp. 357~368, December 1993

Analysis of Undertow Using κ-ε Turbulence Model
k-ε 亂流 模型을 이용한 海向底流의 解析

Seung Yong Hwang* and Kil Seong Lee*
황승용* · 이길성*

Abstract □ With the assumption of the diffusion dominated flow, a numerical model has been developed for undertow and turbulence structure under the breaking wave by using the k-ε turbulence model. Undertow is a strong mean current which moves seqwards below the level of wave trough in the surf zone. The turbulence, generated by wave breaking in the roller, spreads and dissipates downwards. The governing equations are composed of the equation of motion with the period-averaged shear stress due to waves; k- and ε-equations with the turbulence energy production due to wave breaking. They are discretised by the three-level fully implicit scheme, which can be solved by using Thomas algorithm. The model gives good agreements with measurements except for the station that is closest to the breaking point.

要 旨 : 확산이 지배적인 흐름을 가정하여, 쇄파대의 해향저류와 난류구조에 대한 수치모형이 k-ε 난류모형을 이용하여 개발되었다. 해향저류란 쇄파대에서 바다쪽으로 흐르는 주기평균된 강한 흐름을 말하며, 주로 파곡 아래에 나타난다. 롤러에서 쇄파에 의해 발생된 난류는 아래쪽으로 퍼져나가면서 그 기운을 잃게된다. 지배 방정식은 파에 의한 주기평균-전단응력이 고려된 운동 방정식과 쇄파에 의한 난류 에너지 생성이 포함된 k-와 ε-식으로 구성된다. 이 식들은 삼단계 완전 음해법으로 차분되고, Thomas 알고리즘으로 풀 수 있다. 쇄파지점에 가까운 곳을 제외하면, 모형은 실험값과 좋은 일치를 보여준다.

1. INTRODUCTION

The formation of longshore bars has been an interest to coastal engineers but no coherent explanation has been given for this phenomenon. Undertow, seawards bottom current in the surf zone, is one of the most plausible explanations for the formation of longshore bars. Outside the surf zone, the bottom current is reversed. The first qualitative consideration of the phenomenon was given by Dyhr-Nielsen and Sørensen (1970). They described the mechanism for the phenomenon as an on/offshore variation in the mean bottom shear stress from the equilibrium considerations in the moments. The experiments of Longuet-Higgins (1983) also showed that the consequent convergence of two bottom currents could contribute to building up the longshore bar. Fig. 1 shows this explanation for the formation of longshore bars. Other experiments related to undertow have been carried out by Stive (1980); Stive and Wind (1982); Wang *et al.* (1982); Nadaoka and Kondoh (1982); Hansen and Svendsen (1984); Hattori and Aono (1985); Okayasu *et al.* (1988); and Lee and Park (1992).

Dally (1980) first proposed a mathematical model for the description of undertow and quantified the on/offshore gradient of radiation stress and the set-up.

Svendsen (1984b) estimated the vertical distribution of undertow based on the assumptions for waves and their particle velocities as had been used in his previous work (Svendsen, 1984a). He derived formulae for undertow by assuming constant and exponential eddy viscosity distributions in time-averaged momentum equation and compared the calculated undertow profiles with the measurements

*서울대학교 토목공학과 (Department of Civil Engineering, Seoul National University, Seoul 151-742, Korea)

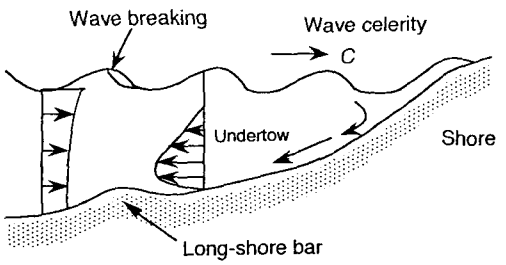

Fig. 1. Formation of long-shore bars.

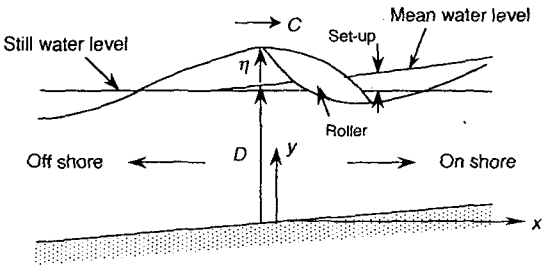

Fig. 2. Definition sketch.

by Stive and Wind (1982). He concluded that the best agreement occurred for the exponentially decaying eddy viscosity.

Svendsen (1987a) analyzed the structure of surf zone turbulence using some experimental data. For turbulence energy dissipation, he concluded that only a very small portion of the total turbulence energy produced was dissipated below the wave trough level.

Deigaard *et al.* (1986) described the vertical distribution of suspended sediment by a one-equation turbulence model under the broken waves. They suggested the energy production due to wave breaking based on the experiments of other researchers. They assumed the distribution of turbulence length scale as a linear variation with the distance from the bed. Svendsen (1987b) raised a question in the discrepancy between time-averaged turbulence kinetic energy measured by Stive and Wind (1982) and the one calculated by Deigaard *et al.* (1986). He pointed out that this discrepancy originated from a too small estimate of length scale (Svendsen, 1987 a).

Deigaard *et al.* (1991) applied their previous model (Deigaard *et al.*, 1986) to undertow and discussed the modeling of turbulence in spilling breakers. They used the coefficient of turbulence length scale (maximum length scale) as a parameter, but the variation of length scale was still linear.

Lee and Park (1993) developed a mathematical model for undertow in which the wave profile in the surf zone was approximated by using the Chebyshev polynomials of the first kind. They compared their results with measurements for constant, linear, and exponential distributions of eddy viscosity; and concluded that the best agreement was obtained for the linear distribution of eddy viscosity.

The goal of the present work is to develop a numerical model for undertow by using κ-ε turbulence model under the turbulence generated due to oscillatory wave boundary layer and wave-breaking process. Two-equation models account for the transport not only of kinetic energy but also of length scale; *e.g.*, turbulence energy dissipation rate for κ-ε model. The k-ε model is one of the simplest models that promise success for flows for which the length scale cannot be prescribed empirically in an easy way (Rodi, 1980). Therefore, it is expected that the present model can eliminate the length scale problem.

2. MATHEMATICAL MODEL

2.1 Governing Equations

The governing equations consist of the equation of motion with the distribution of period-averaged shear stress, continuity equation that balances the shoreward discharge with offshore current, and κ-ε equations that describe the turbulence driven by the wave breaking and boundary layer. The definition sketch of coordinates and variables is shown in Fig. 2.

2.1.1 Equation of motion

If the convective terms are neglected (from the assumption of diffusion dominated flow) and the horizontal diffusion term is also discarded (from the shallow water wave theory that the wave length L, as a horizontal length scale, is much larger than the mean water depth D, as a vertical length scale), the horizontal time-averaged (or by the Reynolds averaging) flow equation can be written as

$$\frac{\partial U}{\partial t}=-\frac{1}{\rho}\frac{\partial p}{\partial x}+\frac{\partial}{\partial y}\left(\nu_t\frac{\partial U}{\partial y}-\frac{\bar{\tau}}{\rho}\right) \tag{1}$$

in which t is the time coordinate, x is the horizontal coordinate, y is the vertical coordinate directed upward from the bed, U is the mean horizontal flow velocity, p is the hydrodynamic pressure, ρ is the density of fluid, ν_t is the eddy (turbulent) viscosity, and $\bar{\tau}$ is the period-averaged shear stress (see next section, for details). The periodic pressure gradient in the flow equation is connected to the horizontal wave orbital velocity u_o:

$$\frac{1}{\rho}\frac{\partial p}{\partial x}=-\frac{\partial u_o}{\partial t} \tag{2}$$

By substituting the above relation, the equation of motion can be modified as follows:

$$\frac{\partial U}{\partial t}=\frac{\partial}{\partial y}\left(\nu_t\frac{\partial U}{\partial y}\right)+\frac{\partial u_o}{\partial t}-\frac{1}{\rho}\frac{\partial \bar{\tau}}{\partial y} \tag{3}$$

2.1.2 Period-averaged shear stress

From equilibrium considerations in the moments, Dyhr-Nielsen and Sφrensen (1970) found an inconsistency between the gradients of radiation stresses and wave set-up and proposed an on/offshore variation in the mean shear stress in surf zone. Dally (1980) quantified the difference through a mathematical derivation. Deigaard and Fredsφe (1989) proposed the modified shear stress distribution for dissipative water waves described using the linear shallow water theory.

A period-averaged shear stress is introduced to obtain an equilibrium in the moments. It consists of the contributions of wave motion, surface roller, and set-up for a steady circulation current (see Deigaard and Fredsφe (1989) for its derivation):

$$\bar{\tau}=-\frac{1}{C}\frac{\partial E_f}{\partial x}\left(1+\frac{D-y}{2D}\right)-\rho gS(D-y)-\frac{\rho}{T}\frac{\partial}{\partial x}(AC) \tag{4}$$

in which E_f is the mean energy flux of wave motion, S is the gradient of setup, T is the wave period, C is the wave celerity, and A is the cross sectional area of each surface roller. Svendsen (1984a) suggested approximate formulae for A and E_f as follows:

$$A\cong 0.9H^2 \tag{5}$$

and

$$E_f\cong B_o\rho gCH^2+0.45\rho\frac{(CH)^2}{T} \tag{6}$$

in which g is the gravitational acceleration, H is the wave height, and B_0 is defined by

$$B_0\equiv\frac{1}{T}\int_{t_0}^{t_0+T}\left(\frac{\eta}{H}\right)^2dt \tag{7}$$

in which η is the water surface elevation measured above the mean water level. For a saw-tooth wave profile, in which a length of the wave front is one quarter of the entire wave length, the value of B_0 is equal to 1/12, which is employed in the present work.

A triangular distribution of the period-averaged shear stress is employed in the present work, according to Deigaard *et al.* (1991). It is adjusted from the wave trough level so that it decreases linearly to be zero at the mean water level. Under the wave trough level, the distribution of period-averaged shear stress is calculated by Eq. (4).

2.1.3. Equation of continuity

From the conservation of mass, the total mass flow, which is taken as a mean over a wave period, must be zero in the two-dimensional steady surf zone. Thus, the mass drift shoreward compensates the depth-integrated offshore period-averaged flow:

$$\int_{y0}^{D}\tilde{U}dy=-Q_{drift} \tag{8}$$

in which $\tilde{U}$ is the period-averaged mean horizontal flow velocity (or undertow) and y_0 is the bed level where the velocity is zero from the log law (see Eq. 18). The mass drift, Q_{drift} consists of two parts: the mass drift due to the wave orbital motion and the contribution of surface rollers (see Svendsen (1984b) for details):

$$Q_{drift}=B_0\frac{CH^2}{D}+\frac{A}{T} \tag{9}$$

In the formula for period-averaged shear stress, the contribution of set-up is dominant below the wave trough level (see Deigaard and Fredsφe (1989) for the graphical comparison of each term). In the present simulation, the gradient of set-up is determined when the mass balance is satisfied.

Table 1. Empirical constants of the k-ε model

Constant	σ_κ	σ_ε	C_0	C_1	C_2
Value	1.00	1.30	0.09	1.44	1.92

2.1.4 k- and ε-equations

Standard k-ε model has two transport equations: turbulence kinetic energy k and its dissipation rate ε. Like the equation of motion, those equations are also linearized by neglecting convection and horizontal diffusion terms. The k-equation is of the form:

$$\frac{\partial k}{\partial t}=\frac{\partial}{\partial y}\left(\frac{\nu_t}{\sigma_k}\frac{\partial k}{\partial y}\right)+P_m+P_b-\varepsilon \tag{10}$$

and ε-equation is of the form:

$$\frac{\partial \varepsilon}{\partial t}=\frac{\partial}{\partial y}\left(\frac{\nu_t}{\sigma_\varepsilon}\frac{\partial \varepsilon}{\partial y}\right)+C_1(P_m+P_b)\frac{\varepsilon}{k}-C_2\frac{\varepsilon^2}{k} \tag{11}$$

in which P_b is the turbulence energy production due to wave breaking (see the next section for details) and turbulence energy production from the mean flow, P_m is of the form in this case

$$P_m=\nu_t\left(\frac{\partial U}{\partial y}\right)^2 \tag{12}$$

From Kolmogorov-Prandtl relationship, the eddy viscosity is estimated by

$$\nu_t=C_o\frac{k^2}{\varepsilon} \tag{13}$$

The empirical constants, i.e., σ_k, σ_ε, C_0, C_1, and C_2 are summarized in Table 1 in accordance with Launder and Spalding (1972).

2.1.5 Energy production due to wave breaking

The generation of turbulence is initiated at the toe of the breaking wave front; the main part of the production of turbulence energy is considered to take place inside or in the nearest proximity of the recirculating water volume, termed the roller, which is carried with the front of the wave (Svendsen, 1987a). The turbulence generated by wave breaking spreads downward from the vicinity of the surface roller so that a substantial amount of turbulence kinetic energy is present over all levels between bottom and surface. Deigaard *et al.* (1986) suggested the following energy production as an analytical approximation based on experiments:

$$P_b=\begin{cases}\alpha_{br}\dfrac{T}{\rho}\dfrac{dE_f}{dx}\dfrac{36}{(H\delta T)^2}z\left(1-\dfrac{z}{H}\right)t\left(1-\dfrac{t}{\delta T}\right), \\ \quad \text{if } 0\le t<\delta T \text{ and } 0\le z<H \\ 0, \qquad \text{otherwise}\end{cases} \tag{14}$$

in which z is the vertical coordinate directed downwards from the mean water level, α_{br} is the turbulence production coefficient (see section 4.1, for its definition), and δ is the part of the total time during which production of turbulence energy takes place:

$$\delta=2\left\{\frac{D+(H/2)}{L}\right\} \tag{15}$$

2.2 Boundary Conditions

For convenience, ϕ is introduced as a certain dependent variable in the governing equations.

At the water surface, no-flux condition is applied:

$$\left.\frac{\partial \phi}{\partial y}\right|_{y=D}=0 \tag{16}$$

in which $\phi=\{U, k, \varepsilon\}$.

From the periodicity in solutions,

$$\phi(y, t)=\phi(y, t+T) \tag{17}$$

At the bed, no-slip condition for the flow velocity is applied:

$$U(y_0, t)=0 \tag{18}$$

in which y_0 is defined by using the Nikuradse sand roughness k_N:

$$y_0=\frac{k_N}{30} \tag{19}$$

The bottom boundary conditions for turbulence kinetic energy and its dissipation rate are assumed as follows:

$$k(y_0, t)=\frac{u_*^2}{\sqrt{C_0}} \tag{20}$$

and

$$\varepsilon(y_0, t)=\frac{u_*^3}{\kappa y} \tag{21}$$

in which κ is the von Kármán constant and u_* is the shear velocity.

3. NUMERICAL MODEL

3.1 Method of Solution

For turbulent flow, the fully implicit scheme has been gaining in popularity since the Crank-Nicolson scheme has occasionally been found to become unstable (Anderson *et al.*, 1984). In the present model, three partial differential equations (Eq. 3, 10, and 11) are discretised by the three-level fully implicit scheme in the finite difference method. This scheme has a truncation error of $O(\Delta t^2, \Delta y^2)$, which is unconditionally stable. The use of the three-level fully implicit scheme leads to a tridiagonal matrix, which can be solved by using the Thomas algorithm. Δt and Δy are grid sizes in time and space coordinates in the computational domain. Three-level fully implicit scheme damps out the spurious oscillations that often appear in the Crank-Nicolson scheme (Richtmyer and Morton, 1967; Fletcher, 1988).

Three-level schemes require two levels to known data; therefore, they must be supplemented at the start of the integration. This should be done with a two-level scheme that achieves the same or better accuracy. Thus, a second-order two-level scheme like the Crank-Nicolson scheme is appropriate.

3.2 Difference Equations

The one-dimensional diffusion equation with a source term can be written for ϕ:

$$\frac{\partial \phi}{\partial t} = \frac{\partial}{\partial y}\left(\frac{\nu_t}{\sigma_\phi}\frac{\partial \phi}{\partial y}\right) + S_\phi \tag{22}$$

in whic σ_ϕ is Prandtl number for ϕ. In the case of $\phi = U$, σ_U is equal to unity and

$$S_U = \frac{\partial u_0}{\partial t} - \frac{1}{\rho}\frac{\partial \bar{\tau}}{\partial y} \tag{23}$$

For convenience, ϕ is used again as a grid function in the computational domain. Using the generalized three-level scheme, the difference equation for Eq. (22) can be written as follows:

$$(1+\alpha)\frac{\phi_j^{n+1}-\phi_j^n}{\Delta t} - \alpha\frac{\phi_j^n-\phi_j^{n-1}}{\Delta t} = (1-\beta)\left\{\frac{\partial}{\partial y}\left(\frac{\nu_t}{\sigma_\phi}\frac{\partial \phi}{\partial y}\right)\right\}^n + \beta\left\{\frac{\partial}{\partial y}\left(\frac{\nu_t}{\sigma_\phi}\frac{\partial \phi}{\partial y}\right)\right\}^{n+1} + S_\phi \tag{24}$$

in which n and j are time and space coordinates in computational domain; α and β are parameters controlling the level and the degree of implicitness, respectively. If $\alpha=0$ and $\beta=1.0$, the fully implicit scheme can be obtained; if $\alpha=0$ and $\beta=0.5$, the Crank-Nicolson scheme can be obtained. A particularly effective three-level scheme is given by the choice: $\alpha=0.5$, $\beta=1.0$. This scheme is referred as the three-level fully implicit scheme (Fletcher, 1988). The diffusion term is approximated by the following finite difference formula:

$$\left\{\frac{\partial}{\partial y}\left(\frac{\nu_t}{\sigma_\phi}\frac{\partial \phi}{\partial y}\right)\right\} \cong \frac{1}{\sigma_\phi}\left\{\frac{\nu_t^+}{\Delta y}\left(\frac{\phi_{j+1}-\phi_j}{\Delta y}\right) - \frac{\nu_t^-}{\Delta y}\left(\frac{\phi_j-\phi_{j-1}}{\Delta y}\right)\right\} \tag{25}$$

in which ν_t^+ and ν_t^- are given by

$$\nu_t^+ = \frac{1}{2}(\nu_{tj+1}+\nu_{tj}) \tag{26}$$

$$\nu_t^- = \frac{1}{2}(\nu_{tj}+\nu_{tj-1}) \tag{27}$$

3.3 Treatment of Nonlinear Terms

The k- and ε-equations have nonlinear terms. These nonlinear terms must be linearized to get the proper solutions (*e.g.*, k and ε have always positive values) because finite difference equations are solved by the techniques for linear algebraic equations. In the present work, the strategy, lagging the coefficients, is applied to the eddy viscosity in the diffusion term and source terms in the k- and ε-equations. This strategy allows to solve the governing equations in an uncoupled manner.

The source terms may be assumed as follows:

$$S_\phi = S_c + S_n\phi^{n+1} \tag{28}$$

in which S_ϕ is the source term in a ϕ-equation. It is noted that the quantity S_c must not be negative, while S_n must not be positive. It is vital to keep S_n negative so that instabilities and physically un-

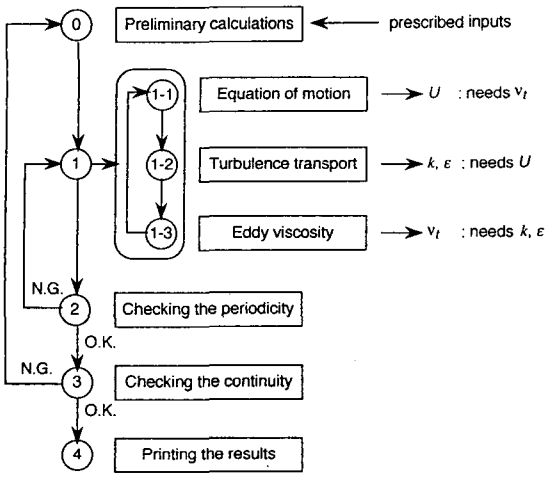

Fig. 3. Solution procedure of the numerical model.

realistic solutions do not arise (Patankar, 1980). In the present work, source terms in k- and ε-equations are employed as follows:

$$S_k = S_c + S_n k_j^{n+1}, \text{ with } S_c = (P_m + P_b)_j^n \text{ and } S_n = -\frac{\varepsilon_j^n}{k_j^n} \tag{29}$$

and

$$S_\varepsilon = S_c + S_n \varepsilon_j^{n+1}, \text{ with } S_c = C_1 (P_m + P_b)_j^n \frac{\varepsilon_j^n}{\kappa_j^n}$$

$$\text{and } S_n = -C_2 \frac{\varepsilon_j^n}{\kappa_j^n} \tag{30}$$

3.4 Solution Procedure

As mentioned in the previous section, governing equations are solved in an uncoupled manner. Fig. 3 schematizes the solution procedure used in present work. That solution procedure can be summarized as follows:

0. Preliminary calculations: wave and period-averaged shear stress profiles are calculated from the input wave data.

1. Solving equations: tri-diagonal matrix is made for each equation in each time step and solved by the Thomas algorithm. Upon computing for two wave periods, maximum relative errors of U, k, and ε are obtained, respectively at each time step. The final maximum error to be used in the test of periodicity is the largest one of the maximum relative errors of U, k, and ε calculated at each time step.

2. Test of periodicity: If the final maximum error is not tolerable, the previous step (1) will be repeated until periodic solutions are retained.

3. Test of continuity: The golden section method searches for the optimal gradient of set-up which gives the best satisfaction for the mass balance (Eq. 8). If a tolerable relative error for the mass balance is obtained, the results will be printed; if not, the above steps (0, 1, and 2) will be repeated with a newly suggested gradient of set-up.

4. MODEL RESULTS

The computational domain is assumed rectangular and divided into fifty grid points from y_0 to D by one hundred grid points in a wave period. The initial values of mean velocity are assumed to be zero; those of k and ε are set to be slightly larger than zero.

The results of the model are compared with some experiments from the literature: the test of Stive (1980), Hansen and Svendsen (1984), and Okayasu *et al.* (1988); in their figures, denoted by ST, HS, and OK, respectively.

4.1 Model Inputs

The present model needs six prescribed input values: mean water depth D, bed roughness k_N, period T, wave height H, and bed slope are given from the geometric properties and wave characteristics for each case; the turbulence production coefficient α_{br} is estimated as a model calibration parameter. The roughness of bed is assumed to be $k_N = 1$ mm for all cases because of the absence of their information.

The turbulence production coefficient, which is expected to be in the range of 0.1~0.5 based on experiments, is defined by the ratio between the production of turbulence and the rate of wave energy loss (Deigaard *et al.*, 1991). They assumed that the surface roller could be considered as a shear layer where a large part of the wave energy loss is converted into turbulence, which is dissipated immediately, and only a minor part is transported

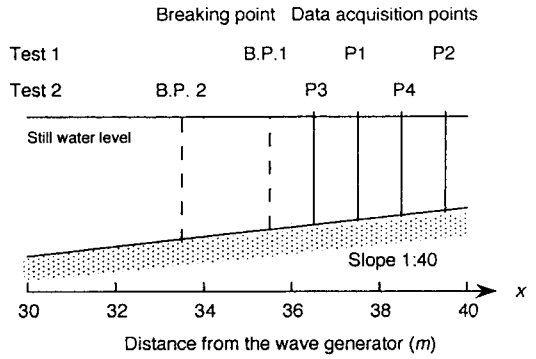

Fig. 4. Experiments of Stive (1980).

away by convection and diffusion.

The gradient of set-up S is dominant contribution in the period-averaged shear stresses. It is chosen to be slightly larger value than necessary to balance the radiation stress gradient, giving a negative mean bed shear stress and an offshore directed flow near the bed (Deigaard *et al.*, 1991).

In the present simulation, the golden section search method is used to obtain the optimal gradient of set-up satisfying the mass balance automatically. The golden section search method is one of the simplest techniques to minimize a function of one variable, or the relative error for mass balance which is a function of the gradient of set-up. The method is not an essential part of the present work, but gives an easier and more precise estimation than a trial and error method does; in the present simulation, the values of relative errors were in the range of 0.0055~0.0897% for all cases.

4.2 Model Calibration

The measurements of Stive (1980) were selected as model calibration data. In the test, the wave broke on a plane and concrete beach of a 1:40 slope and two series of tests have been made: in test 1, the wave period, $T=1.79$ sec and the deep water wave height, $H_0=0.159$ m; in test 2, $T=3.00$ sec and $H_0=0.142$ m. They measured the velocity components by using an LDA (Laser Doppler Anemometer). Data acquisition points and input values are summarized in Fig. 4 and Table 2, respectively.

4.2.1 Estimation of the model parameter α_{br}

The model has been run for various turbulence production coefficients α_{br}. Comparisons with the measurements of turbulence kinetic energy of Stive (1980) are shown in Fig. 5. In the figure, circles and curves represent measured and calculated values, respectively.

Table 2. Measurements at data acquisition points (Stive, 1980)

Points	D	H	Remark
P1	0.162m	0.081	Test 1
P2	0.122m	0.055m	Test 1
P3	0.186m	0.101m	Test 2
P4	0.143m	0.080m	Test 2

The results of Deigaard *et al.* (1991) had the best agreements with the measurements of Stive (1980) when $\alpha_{br}=0.3$. However, Svendsen (1987a; 1987b) argued against their estimation through the analysis of measurements in the surf zone turbulence and concluded that only 2~6% of the total turbulence energy production would be dissipated below trough level. This amount is much smaller than the value estimated by them. In the present simulation, the best agreement with measurements was found when $\alpha_{br}=0.1$ which is a lower limit of it. Fig. 5 shows turbulence kinetic energy profiles at P2 when $\alpha_{br}=0.1$, 0.2, and 0.3. The calculated profile is shifted to the right as α_{br} increases. For other cases, the profiles also showed the same trends.

4.2.2 Comparison of length scales

The model of Deigaard *et al.* (1991) has another parameter, which is the maximum length scale, l_{max}. They used a formula for the length scale as follows:

$$l=\begin{cases} \sqrt[4]{C_D}\kappa y & \text{for } y<\dfrac{l_{max}}{\sqrt[4]{C_D}\kappa} \\ l_{max} & \text{for } y>\dfrac{l_{max}}{\sqrt[4]{C_D}\kappa} \end{cases} \tag{30}$$

in which C_D is an empirical constant for turbulence. They used a value of $C_D=0.08$.

They chose l_{max} of $0.07D$ through the comparison with experiments of Stive (1980). This value is much smaller than that estimated by Svendsen (Svendsen, 1987a), and about $0.2D$~$0.3D$ from the test of Stive. Furthermore, they considered the length scale as a calibration parameter, though it must be determined through the experiments. The application of

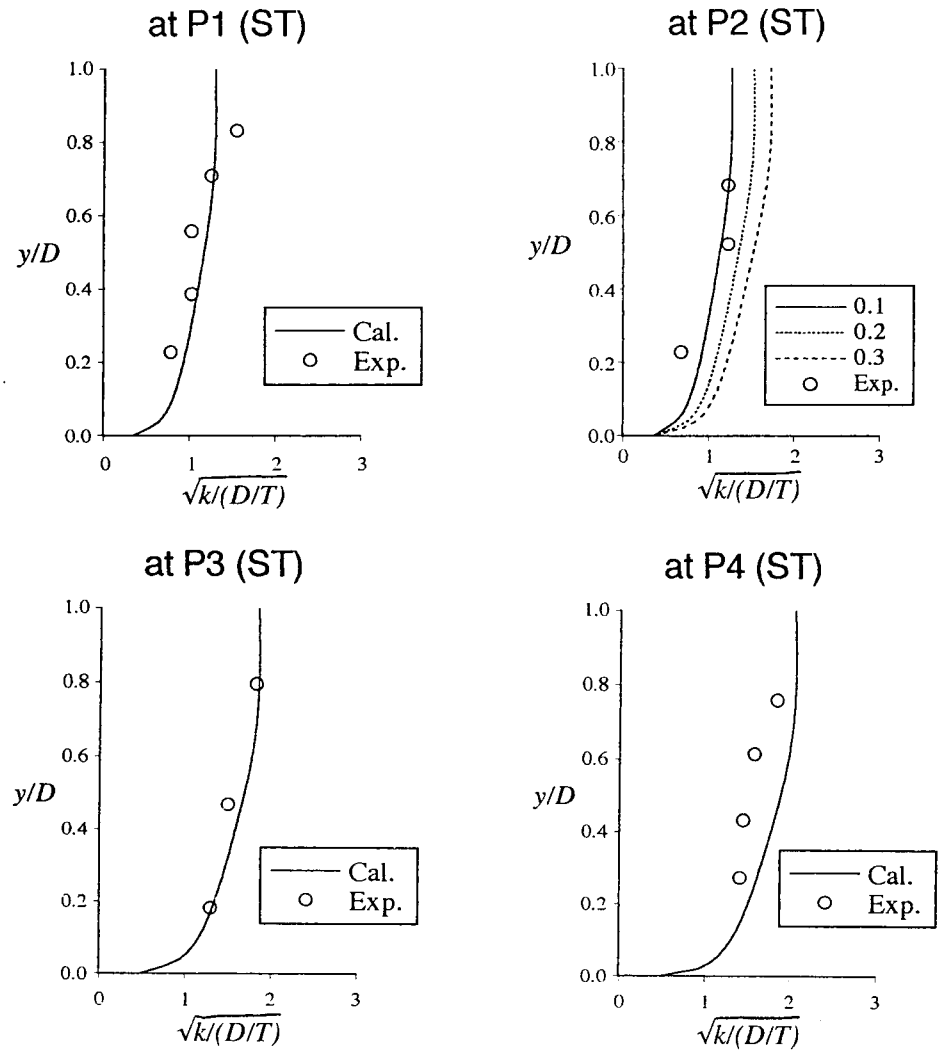

Fig. 5. Calculated and measured period-averaged turbulence kinetic energy profiles in the test of Stive (1980).

one-equation models was restricted mainly to shear layer since it is difficult to specify empirically the length scale distribution in more complex flows; therefore, the trend has been to move on to two-equation models that determine the length scale from a transport equation (Rodi, 1980).

In the present model, no parameter is needed for the length scale as mentioned in the introduction. Fig. 6 shows the comparison between their length scale profile and the calculated one in the present model. The present model gives more natural distribution of the length scale, which is about two times larger than that used by them except for the results near the bed.

4.3 Model Verification

Model verification studies were made by using the measurements of Hansen and Svendsen (1984) and Okayasu *et al.* (1988). In both cases, the model parameter $\alpha_{br}=0.1$ was used.

4.3.1 Comparison with the test of Hansen and Svendsen (1984)

Hansen and Svendsen (1984) carried out experiments in a flume with a plane beach sloping 1:34.25. They measured the particle velocities using a bidirectional micro-propeller current meter. The

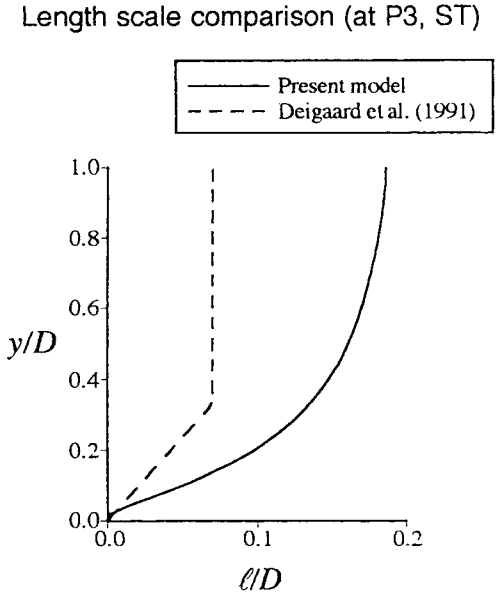

Fig. 6. Comparison of length scale profiles at P3 in the test of Stive (1980).

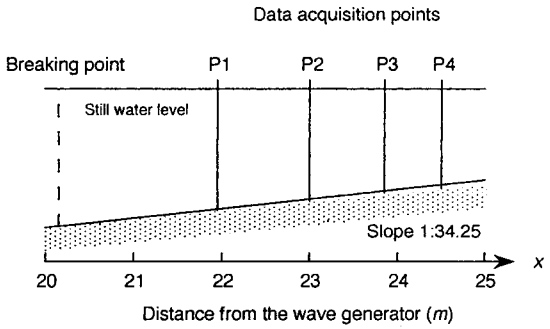

Fig. 7. Experiments of Hansen and Svendsen (1984).

Table 3. Measurements at data acquisition points (Hansen and Svendsen, 1984)

Points	D	H
p1	0.148m	0.111m
P2	0.123m	0.081m
P3	0.102m	0.067m
P4	0.087m	0.052m

wave conditions were the wave period, $T=2.00$ sec and the deep water wave height, $H_0=0.12$ m. Data acquisition points and input values are summarized in Fig. 7 and Table 3, respectively.

Fig. 8 shows comparisons of calculated and measured undertow profiles at four data acquisition points after breaking. It is seen that there is a good agreement between measured and calculated undertow profiles.

At P1 which is closest to the breaking point, however, the agreement is less good. This result may be explained as an inaccurate estimation of onshore mass drift near the breaking point. Svendsen made a crude simplification (see Svendsen (1984a) for its derivation) in the derivation of mass drift (Eq. 9). This simplification may give a worse result near the breaking point. As mentioned in section 4.1, the present model finds the value of the gradient of set-up that gives the best satisfaction for the mass balance. If the estimation of mass drift, which compensates the discharge of the offshore current, is poor, the calculated undertow profile will not be guaranteed for its accuracy. The mass balance was not always satisfied in the case of the best agreements with experiments; but there is not yet another alternative. All the results shown in the figure are the profiles that give the best satisfactions for the mass balance.

4.3.2 Comparison with the test of Okayasu *et al.* (1988)

The model results were also compared with the measurements of Okayasu *et al.* (1988). They measured the velocity fields by using a two-component LDA for 10 different cases. Case 2 was selected for comparison with calculated values. The breaking point in Case 2 is 2 m from the shoreline: the wave period, $T=2.00$ sec and the deep water wave height, $H_0=0.056$ m. Data acquisition points and input values are summarized in Fig. 9 and Table 4, respectively.

The comparisons with measurements for undertow are depicted in Fig. 10. At point P1, the calculated profile is rather underestimated; at P2, the agreement with measurements is satisfactory.

Okayasu *et al.* (1988) calculated the mean Reynolds stresses and the eddy viscosity distributions from the measured turbulent velocity components and the eddy viscosity model in Case 2 and estimated the distributions of Reynolds stresses and eddy viscosity by using the linear regression analysis.

Fig. 11 shows the comparisons between calculated (by the present model), measured (or calculated by

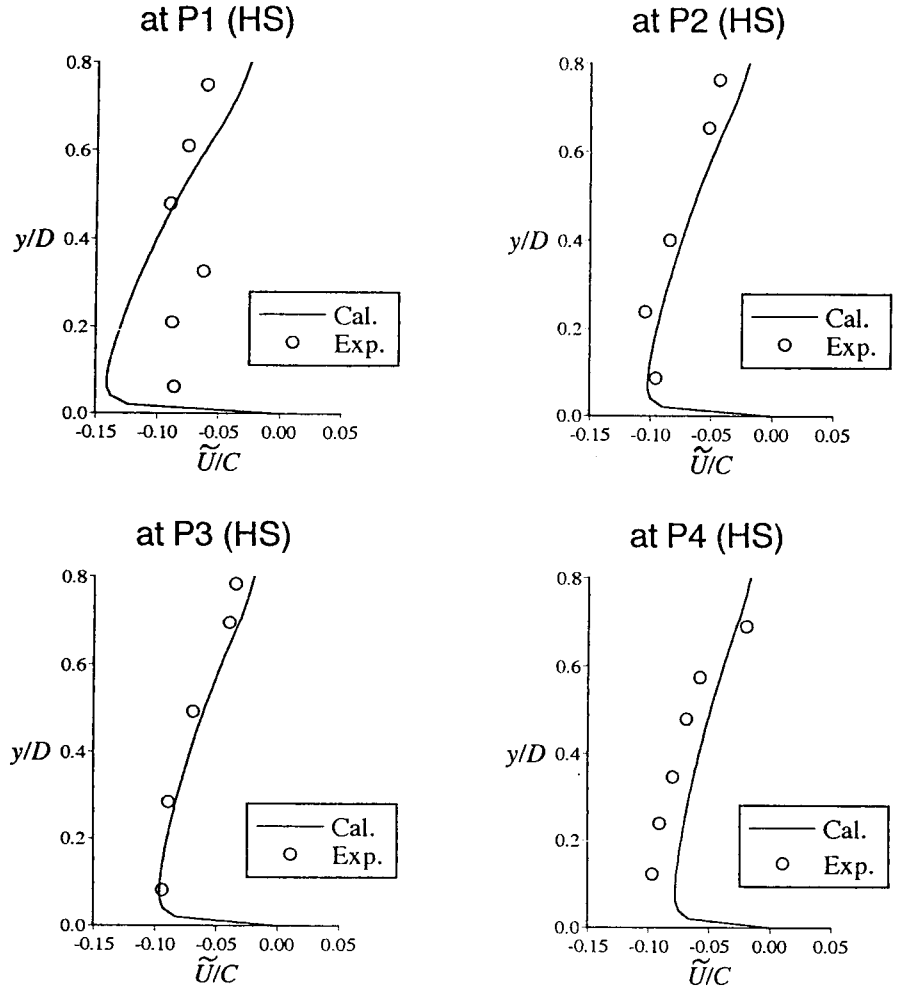

Fig. 8. Calculated and measured undertow profiles in the test of Hansen and Svendsen (1984).

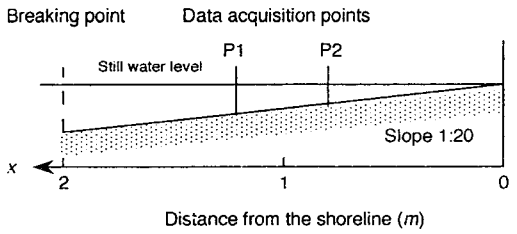

Fig. 9. Experiments of Okayasu *et al.* (1988).

Table 4. Measurements at data acquisition points (Okayasu *et al.*, 1988)

Points	D	H
P1	0.071m	0.050m
P2	0.040m	0.028m

Okayasu *et al.*) and estimated (by Okayasu *et al.*; see Okayasu *et al.* (1988) for their derivations) eddy viscosity and shear stress distributions at point P2. In the figures, broken lines represent the values estimated by regression analysis.

As shown in Fig. 11, the eddy viscosity profile is over-predicted by the model. The distribution of measured one is very irregular. In the present model, the eddy viscosity is calculated by using the Kolmogorov-Plandtl relation (Eq. 13) between the turbulent kinetic energy and its dissipation rate which are solutions of their parabolic partial differential equations in one-dimension. It is very difficult to predict well such irregular behaviors in one-

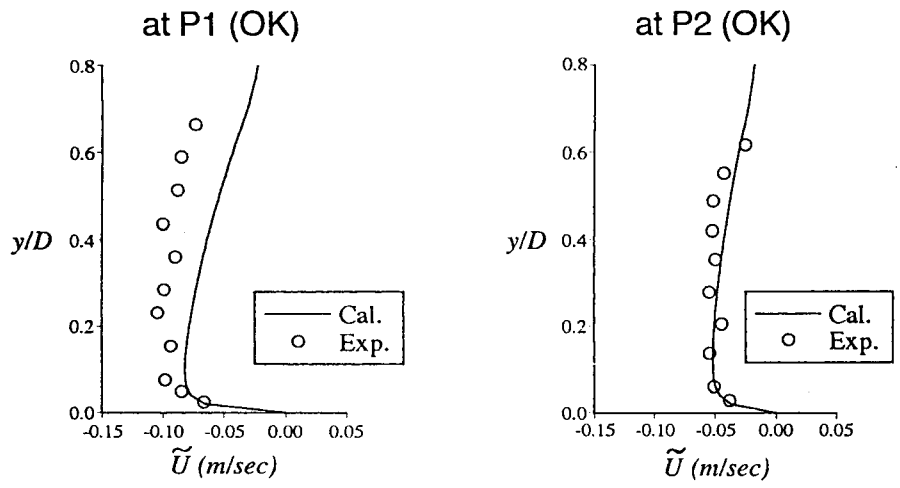

Fig. 10. Calculated and measured undertow profiles in the test of Okayasu *et al.* (1988).

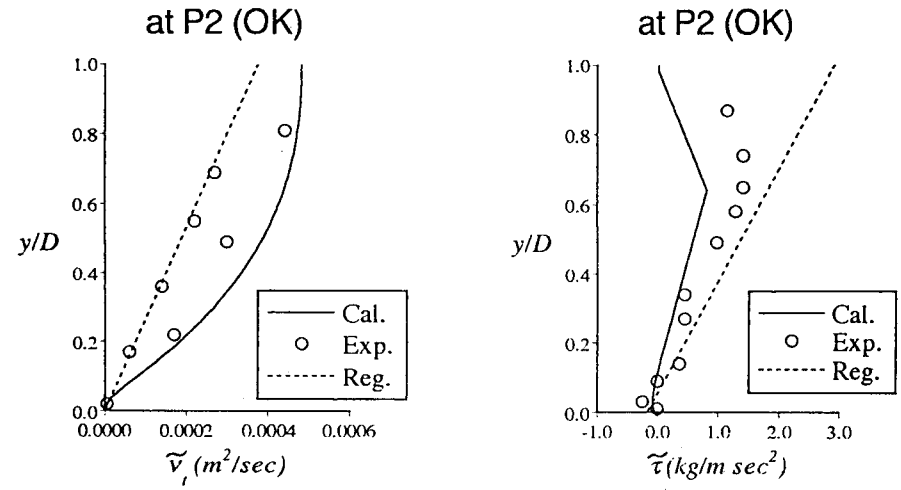

Fig. 11. Calculated and measured eddy viscosity and shear stress profiles at P2 in the test of Okayasu *et al.* (1988).

dimensional computation domain. Thus, it is needed to extend to the complete two- or three-dimensional models.

The present model calculates the shear stress from the relation between eddy viscosity and mean velocity gradient. In the figure, the unrealistic distribution of shear stress near the wave trough level originates in the triangular distribution of period-averaged shear stress (as mentioned in section 2.1.2) which influences flow field, or mean velocity gradient as a strong driving force. The assumption, made by Deigaard *et al.*, has questionable applicability to the region above the trough level; however, the distribution is acceptable in the region where undertow is found actually, below the trough level.

5. CONCLUSIONS

The conclusions can be summarized as follows:

1. With the assumption of the diffusion dominated flow, a numerical model has been developed for undertow and turbulence structure under the breaking wave by using a k-ε turbulence model. The governing equations were discretised by the three-level fully implicit scheme, one of finite difference methods.

2. In the model calibration study, the model calibration parameter $\alpha_{br}=0.1$ was obtained. This means that only 10% of turbulence produced at the surface is transported away by convection and diffusion. This estimate is similar to the analysis of turbulence measurements in the surf zone (see Svendsen (1987a)).

3. The determination of the gradient of set-up was obtained by the golden section search method. This strategy gives a more accurate and easier estimation than the trial and error method does.

4. The present model gives good agreements with measurements except for the stations near the breaking point. The model explains well the existence of a strong mean current, undertow.

The following suggestions for future studies can be offered:

1. The errors associated with linearization of coefficients are related to the marching step size. To reduce the truncation errors or marching step size, another linearization strategy may be required.

2. A more accurate estimation of onshore mass drift is needed. This will improve the accuracy of prediction of undertow profile near the breaking point.

3. The variation of wave energy along x-axis is important in evaluating period-averaged shear stress distribution and the energy production due to wave breaking. Turbulence is rotational and three-dimensional. For these reasons, extensions to the complete two- or three-dimensional models are needed. However, computational costs will be increased extremely high.

REFERENCES

Anderson, D.A., Tannehill, J.C. and Pletcher, R.H., 1984. *Computational fluid mechanics and heat transfer.* Hemisphere Publishing Corp., Wash., D.C.

Deigaard, R. and Fredsφe, J., 1989. shear stress distribution in dissipative water waves. *Coastal Eng.,* **13**, pp.357-378.

Deigaard, R., Fredsφe, J. and Hedegaard, I.B., 1986. Suspended sediment in the surf zone. *J. of Waterway, Port, Coastal and Ocean Eng., ASCE,* **112**(1), pp.115-128.

Deigaard, R., Justesen, P. and Fredsφe, J., 1991. Modelling of undertow by a one-equation turbulence model. *Coastal Eng.,* **15**, pp.431-485.

Dally, W.R., 1980. *A numerical model for beach profile evolution.* M.S. Thesis, Univ. of Delaware.

Dyhr-Nielsen, M. and Sφrensen, T., 1970. Some sand transport phenomena on coasts with bars. *Proc. 12th Int. Conf. Coastal Eng.,* Washington, D.C., pp.855-866.

Fletcher, C.A.J., 1988. *Computational techniques for fluid dynamics.* Vol.I, Springer-Verlag, N.Y.

Hansen, J.B. and Svendsen, I.A., 1984. A theoretical and experimental study of undertow. *Proc. 19th Int. Conf. Coastal Eng.,* Houston, pp.2246-2262.

Hattori, M. and Aono, T., 1985. Experimental study on turbulence structures under breaking waves. *Coastal Eng. in Japan,* **28**, pp.97-116.

Launder, B.E. and Spalding, D.B., 1972. *Lectures in mathematical models of turbulence,* Academic Press Inc., N.Y.

Lee, J.S. and Park, I.H., 1992. Hydraulic experiment of wave height dissipation and return flow in the surf zone. *Ann. Meeting Korean Soc. of Coastal and Ocean Eng.,* pp.106-113 (in Korean).

Lee, J.S. and Park, I.H., 1993. A mathematical model of undertow in the surf zone. *Proc. Korean Soc. of Civil Eng.,* **13**(3), pp.193-206 (in Korean).

Longuet-Higgins, M.S., 1983. Wave set-up, percolation and undertow in the surf zone. *Proc. R. Soc. Lond., Ser. A,* **390**, pp.283-291.

Nadaoka, K. and Kondoh, T., 1982. Laboratory measurements of velocity field structure in the surf zone by LDV. *Coastal Eng. in Japan,* **25**, pp.125-145.

Okayasu, A., Shibayama, T. and Horikawa, K., 1988. Vertical variation of undertow in the surf zone. *Proc. 21st Int. Conf. Coastal Eng.,* Costa del Sol, Malaga, Spain, pp.478-491.

Patankar, S.V., 1980. *Numerical heat transfer and fluid flow.* Hemisphere Publishing Corp., Wash., D.C.

Richtmyer, R.D. and Morton, K.W., 1967. *Difference method for initial-value problem.* 2nd Ed., John Wiley & Sons Inc., N.Y.

Rodi, W., 1980. Turbulence models for environmental problems. *Prediction methods for turbulent flow,* Ed. Kollmann, W., Hemisphere Publishing Corp., Wash., D. C.

Stive, M.J.F., 1980. Velocity and pressure field of spilling breakers. *Proc. 17th Int. Conf. Coastal Eng.,* Sydney, pp.547-566.

Stive, M.J.F. and Wind, H.G., 1982. A study of radiation stress and set-up in the nearshore region. *Coastal Eng.,* **6**, pp.1-25.

Svendsen, I.A., 1984a. Wave heights and set-up in a surf zone. *Coastal Eng.,* **8**, pp.303-329.

Svendsen, I.A., 1984b. Mass flux and undertow in a surf zone. *Coastal Eng.,* **8**, pp.347-365.

Svendsen, I.A., 1987a. Analysis of surf zone turbulence. *J. Geophys. Res.,* **92**(C3), pp.5115-5124.

Svendsen, I.A., 1987b. Discussion of 'Suspended sediment in the surf zone' by Deigaard *et al. J. of Waterway, Port, Coastal and Ocean Eng., ASCE,* **113**(5), pp.555-557.

Wang, H., Sunamura, T. and Hwang, P.A., 1982. Drift velocity at the wave breaking point. *Coastal Eng.,* **6**, pp. 121-150.